Effective Synthesis of Single-Walled Carbon Nanotubes Using Ni–MCM-41 Catalytic Template through Chemical Vapor Deposition Method

ARTICLE *in* INDUSTRIAL & ENGINEERING CHEMISTRY RESEARCH · NOVEMBER 2006

Impact Factor: 2.59 · DOI: 10.1021/ie060663a

2 AUTHORS:

Thirunavukkarasu Somanathan
Vels University
34 PUBLICATIONS **145** CITATIONS

SEE PROFILE

Pandurangan Arumugam
Anna University, Chennai
155 PUBLICATIONS **1,881** CITATIONS

SEE PROFILE

Effective Synthesis of Single-Walled Carbon Nanotubes Using Ni−MCM-41 Catalytic Template through Chemical Vapor Deposition Method

Thirunavukkarasu Somanathan[†] and Arumugam Pandurangan*[,†,‡]

Department of Chemistry, Anna University, Chennai 600 025, India, and Center for Applied Energy Research, University of Kentucky, Kentucky 40511-8410

Mesoporous Ni−MCM-41 molecular sieves with various Si/Ni ratios 25, 50, 75, and 100 were synthesized hydrothermally, and their mesoporous structure was confirmed by various physicochemical techniques such as X-ray diffraction (XRD), N_2 adsorption studies, scanning electron microscopy (SEM), and transmission electron microscopy (TEM). The catalytic activity of these molecular sieves was tested and optimized for the maximum yield of carbon nanotubes (CNTs) in the vapor phase at various temperatures ranging from 650 to 850 °C. Ni−MCM-41 (100) was found to consist of the optimum amount of metal to form large metallic clusters leading to higher carbon deposits. The optimum reaction temperature for high carbon deposits was found to be at 750 °C. The maximum percentage of carbon deposit increased from 9.33 to 71.01% when the flow rate was increased from 20 to 60 mL/min. The purified CNTs were characterized by XRD, SEM, TEM, and Raman spectroscopy techniques. The analysis showed that these CNTs have larger diameters and good graphitization. The morphology of CNTs studied by TEM clearly showed the formation of carbon nanotubes with uniform diameter in the range of 25−30 nm.

Introduction

Since the discovery by Iijima in 1991,[1] carbon nanotubes (CNTs) have attracted much attention due to their unique properties and potential applications in numerous areas such as electronic and mechanical devices,[2] hydrogen storage,[3] field emission tips,[4] and nanotweezers.[5] It has been demonstrated that CNTs could store hydrogen electrochemically,[6,7] but with less storage capacity, far from the benchmark system weight efficiency (the ratio of stored hydrogen weight to system weight) of 6.5 wt %, which is put forward by the U.S. Department of Energy (DOE) hydrogen plan.[8] Since the properties of CNTs are expected to be dependent on their diameters and helicity,[9] considerable efforts have been made to study the synthesis and growth mechanism of CNTs.[10,11] CNTs are usually prepared by arc evaporation,[12] laser ablation,[13] or chemical vapor deposition.[14] The catalytic chemical vapor deposition (CCVD) method has been considered one of the most promising techniques for single-walled carbon nanotube (SWNT) synthesis in recent years, due to the possible industrial scaling up of the CCVD process.[15−17] Various CCVD methods are already known for the production of SWNTs by using different carbon precursors.[18−20] Among the carbon sources utilized for SWNT production, CCVD studies with acetylene are limited due to the following reasons.[21−23]

Acetylene is considered a good carbon source for SWNT production because it contains fewer number of carbon atoms per molecule and greater activity in comparison to other hydrocarbons such as benzene.[24] Recently metal-substituted MCM-41 materials have been introduced for the synthesis of SWNTs by Haller and co-workers,[25,26] but they reported a lower yield compared to the results presented here. Synthesis of SWNTs with narrow-diameter distribution is also reported on MgO support material synthesized by incorporating the metal catalyst precursors.[27] If the metal precursor is included within silica or MgO during the support material synthesis, the diameter distribution of SWNTs is observed to be much narrower. This is due to the high dispersion and strong interaction of the metal catalyst with the support materials. Catalysts with large surface area having active catalytic centers are important for the large-scale production of CNTs using CVD method.

In general, MCM-41 and related mesoporous molecular sieves of the M41S family are materials of interest because of their remarkable properties such as large surface (>1000 m^2/g), pore volume (>0.8 cm^3/g), very narrow pore size distribution, and the ease with which their surface can be functionalized.[28] Also, their uniform and tunable pore diameters make them well-adapted as good catalytic supports. Generally, pure silica MCM-41 has limited catalytic activity, but active catalytic sites can be generated in MCM-41 by isomorphously substituting silicon with a metal.[29] Several studies have been dedicated to the investigation of transition-metal-substituted MCM-41 because of their wide range of applications in catalysis.

The use of mesoporous silica rather than a zeolitic material as a catalytic template for the production of CNTs is gaining prominence because of the possibility of controlling the pore diameter independent of the chemical composition of the pore walls. This allows these parameters to be used independently to control the size of the metal particles incorporated in the mesoporous from which the initiation of CNT growth is believed to occur. The metal particle plays an important role during CNT production, and reports abound showing a direct correlation between the size of the metal nanoparticles and the eventual tube diameter.[30] Thus, the ultimate goal of being able to control the diameter of CNTs would require a thorough understanding of the microstructure, stability, and chemical properties of the catalytic template. In the growth of CNTs, dispersion of metal over the support plays an important role for the formation of well-graphitized CNTs. In the present work, we have used Ni−MCM-41 (Si/Ni = 25, 50, 75, and 100) as a catalytic template using acetylene as a carbon precursor for the growth of CNTs in the vapor phase. The results indicate that the metal, which is present at the tip of the nanotubes, follows a tip growth mechanism. The well-graphitized CNTs of about 25−30 nm

* To whom correspondence should be addressed. Tel.: +91-22203158. Fax: +91-44-22200660. E-mail: pandurangan_a@yahoo.com.
[†] Anna University.
[‡] University of Kentucky.

10.1021/ie060663a CCC: $33.50
Published on Web 11/15/2006

formed out of the pores of the MCM-41 mesoporous materials are clearly observed. The purified CNTs were characterized by X-ray diffraction, Scanning electron microscopy (SEM), transmission electron microscopy (TEM), and Raman spectroscopy.

Experimental Section

Materials. The chemicals used for the synthesis of mesoporous molecular sieves were sodium metasilicate (E-Merck) and nickel nitrate (E-Merck). They were the sources of silicon and nickel, respectively. Cetyltrimethylammonium bromide (CTAB; Qualigens) was used as the structure-directing template. Sulfuric acid was used to adjust the pH of the medium.

Synthesis of Ni−MCM-41 Molecular Sieves. Ni−MCM-41 with various ratios (Si/Ni = 25, 50, 75, and 100) was synthesized hydrothermally according to our previous report[31] using a gel composition of 1:*X*:0.2:0.89:120 SiO_2:$Ni(NO_3)_2$:CTAB:H_2SO_4:H_2O.

Synthesis of Carbon Nanotubes. The experiments to produce CNTs were carried out in a horizontal furnace at atmospheric pressure. About 100 mg of the catalyst was spread on a long quartz boat, which was placed inside a quartz tube. The reaction mixture containing acetylene and nitrogen gas was passed over the catalyst bed for a predetermined time. The experiments were carried out at three different temperatures: 650, 750, and 850 °C. The percentage of carbon deposited due to the catalytic decomposition of acetylene was obtained from the following equation:

$$\text{carbon deposit (\%)} = 100 \times (m_{\text{tot.}} - m_{\text{cat.}})/m_{\text{cat.}}$$

where $m_{\text{cat.}}$ and $m_{\text{tot.}}$ are the mass of the catalyst before and after the reaction, respectively. The final product was obtained as a black solid powder and submitted to a purification procedure to eliminate the inorganic materials. The removal of the silica phase was carried out by treating with 40 wt % hydrofluoric acid at ambient temperature as reported in earlier literature.[32] Then the obtained solid product was filtered and washed with distilled water and was subsequently immersed in 6 M HCl to dissolve the metal catalyst. The final product was washed with deionized water, filtered, and dried at 60 °C. The process was monitored by XRD, SEM, TEM, and Raman spectroscopy.

Characterization. The powder XRD patterns of the calcined mesoporous Ni−MCM-41 molecular sieves and CNTs were obtained with a Stereoscan diffractometer using nickel-filtered Cu Kα radiation (λ = 1.5418 Å) and a liquid nitrogen cooled germanium solid-state detector. Surface area, pore volume, and pore size distribution were measured by nitrogen adsorption at 77 K with an ASAP-2010 porosimeter from Micromeritics Corp. (Norcross, GA). The samples were degassed at 623 K at 10^{-5} m bar overnight prior to the adsorption experiments. The mesopore volume was estimated from the amount of nitrogen adsorbed at a relative pressure of 0.4 by assuming that all the mesopores were filled with condensed nitrogen in the normal liquid state. Pore size distribution was estimated using the Barrett, Joyner, and Halenda (BJH) algorithm (ASAP-2010 built-in software from Micromeritics). SEM was performed to analyze the microstructure of CNTs. A Phillips X30 ESEM microscope was used to examine the formation of CNTs. The growth morphology and crystallinity of the tubular structures were confirmed by TEM. For this purpose, a Phillips CM 200 microscope operating at 200 kV was used. The TEM samples were prepared by sonicating a small amount of carbon nanotube sample in ethanol and ultrasonicating for 20 min. After allowing the product to settle down for some time, one drop of the solution was dropped over a holey copper carbon grid and examined at 200 kV. Information about the vibrational properties of the nanostructures was obtained by FT-Raman spectroscopy. The Raman spectra were recorded using an excitation wavelength of 1064 nm of a Nd:YAG Laser.

Table 1. Influence of Catalysts

		flow rate		
catalysts	reacn temp (°C)	nitrogen (mL/min)	acetylene (mL/ min)	carbon deposits (%)
Ni−MCM-41 (25)	650−850	140	40	46.58
Ni−MCM-41 (50)				48.88
Ni−MCM-41 (75)				50.01
Ni−MCM-41 (100)				58.54

Table 2. Influence of Temperature

	flow rate		
reacn temp (°C)	nitrogen (mL/min)	acetylene (mL/min)	carbon deposits (%)
650	140	40	07.75
750			38.57
850			14.17

Result and Discussion

Influence of the Catalysts. The growth of CNTs was carried out using Ni−MCM-41 molecular sieves (Si/Ni = 25, 50, 75, and 100) at various temperatures ranging from 650 to 850 °C for 10 min at the N_2 and C_2H_2 flow rates of 140 and 40 mL/min, respectively. The results are given in Table 1. The activity of the catalysts follows the order Ni−MCM-41 (100) > Ni−MCM-41 (75) > Ni−MCM-41 (50) > Ni−MCM-41 (25). The higher carbon deposits in the presence of Ni−MCM-41 (100) of about 58.54% carbon deposits might be due to its greater ability to decompose unsaturated hydrocarbons such as acetylene, and also this ratio possesses the optimum amount of metal to form large metallic clusters leading to the growth of SWNTs compared to other Si/Ni ratios, where the carbon deposit yields were 46.58, 48.88, and 50.01 for Si/Ni = 25, 50, and 75, respectively. Whether the nickel migrates through the silica framework as anion or a metal atom is not yet understood, and the clarification of this mechanism is beyond the scope of this study. However, once the reduced atoms reach the pore wall surface, they start to nucleate into clusters of increasing size before they initiate the growth of carbon nanotube or other types of carbon on their surface. Both the solubility of carbon into metallic particles[33] and the ability of the particle to dissociate C_2H_2 decrease with the particle size. Under certain reaction conditions, very small metal clusters that are not active for SWNT growth would likely be present in the pores. It should also be noted that we observed that the growth of Ni clusters likely ceases once their surface is covered with carbon. Therefore, the optimum size and the size distribution of the metal clusters are controlled by the relative rates of the several physical and chemical processes affecting the structure and state of the catalysts during the SWNT synthesis. There is likely a minimum size required for the metallic Ni cluster to initiate the growth of a SWNT. Hence, Ni−MCM-41 (100) was chosen to carry out further studies since it gave the maximum yield of carbon deposits.

Influence of Reaction Temperature. The effects of reaction temperature on the yield of carbon deposits are studied, and results are shown in Table 2. The study was conducted through the optimized catalyst Ni−MCM-41 (100) at the nitrogen and acetylene flow rates of 140 and 40 mL/min, respectively, for

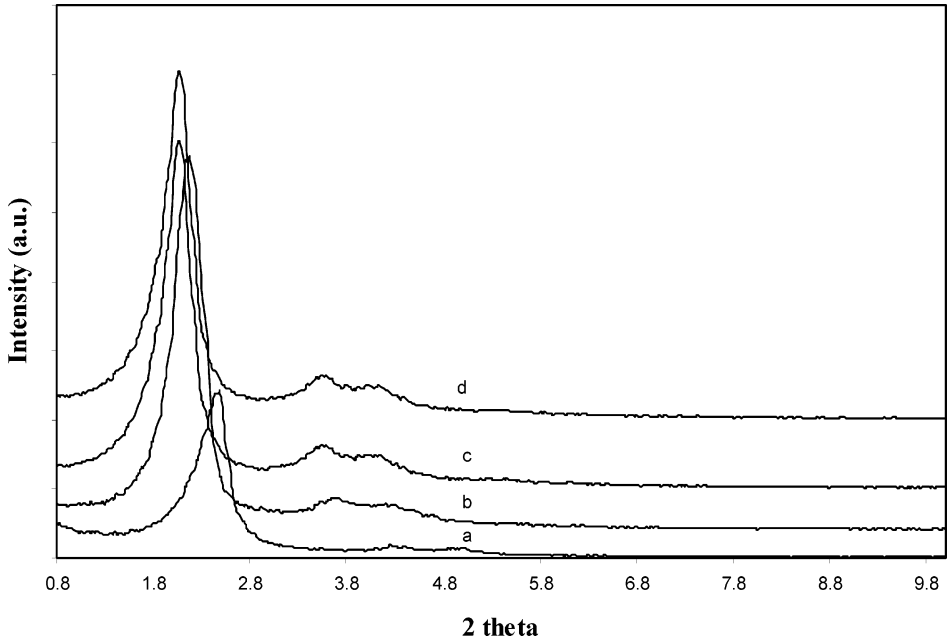

Figure 1. X-ray diffraction patterns of calcined Ni−MCM-41: (a) Ni−MCM-41 (25), (b) Ni−MCM-41 (50), (c) Ni−MCM-41 (75), and (d) Ni−MCM-41 (100).

Table 3. Influence of Flow Rate

flow rate		
nitrogen (mL/min)	acetylene (mL/min)	carbon deposits (%)
140	20	9.33
	30	16.92
	40	42.23
	50	54.36
	60	71.01
	70	70.58
	80	60.84

10 min over the temperatures 650, 750, and 850 °C, and the yields were found to be 7.75, 38.57, and 14.17%, respectively. It is observed that a large amount of multiwalled carbon nanotubes (MWNTs) is synthesized along with SWNTs at 650 °C. The amount of SWNTs is observed to be higher, and very few MWNTs are produced, when the reaction temperature is increased to 750 °C. If the reaction temperature is increased further to 850 °C, more graphitic sheets are found to form apart from SWNTs. From this result, we infer that the interaction between the metal catalyst and MCM-41 is weaker at 650 °C. If this state of the metal catalyst is exposed to acetylene, metal particles can easily diffuse on the surface to form larger particles, leading to MWNT growth. When the reaction temperature reaches 750 °C, the metal−support interaction becomes stronger and stabilizes the nanometer size particles suitable for SWNT growth. However, a higher reaction temperature such as 850 °C leads to the formation of graphitic sheets over MCM-41. Hence, 750 °C was found to be the optimum temperature to grow a high yield of SWNTs with lower amounts of MWNTs and graphitic impurities.

Influence of Flow Rate. Further, the effects of different flow rates on the carbon deposits were studied over the optimized condition, Ni−MCM-41 (100) at 750 °C for 10 min, and the results are presented in Table 3. When the flow rate of acetylene increased from 20 to 80 mL/min, a nonlinear trend in carbon deposits was observed. When the flow rate was increased from 20 to 60 mL/min, we observed a maximum percentage of carbon deposit increasing from 9.33 to 71.01%; then the percentage of carbon deposit decreased to 70.58 and 60.84% when the flow rate further was raised to 70 and 80 mL/min, respectively. This

Table 4. Textural Properties of the Calcined Catalysts (Si/Ni = 25, 50, 75, and 100)

catalysts	d_{100} (Å)	unit cell a_0 (nm)	surface area (m^2/g)	pore size BJH_{Ads} (nm)	pore vol BJH_{Ads} (cm^3/g)
Ni−MCM-41 (100)	42.51	4.90	1023	2.644	0.9575
Ni−MCM-41 (75)	42.55	4.90	1018	2.631	0.9540
Ni−MCM-41 (50)	40.58	4.69	976.6	2.538	0.9407
Ni−MCM-41 (25)	35.39	4.09	950.8	2.501	0.9457

may be due to the decrease in the contact time of the hydrocarbon with an increase in the flow of the carrier gas. Optimizing the reaction condition for maximum carbon deposits yielded 71.01% using Ni−MCM-41 (100) at 750 °C for 10 min at nitrogen and acetylene flow rates of 140 and 60 mL/min.

Characterization of Catalyst and Carbon Nanotubes. (a) XRD. XRD powder diffraction patterns of the mesoporous catalysts as shown in Figure 1, and Table 4 shows an intense diffraction peak at 2.2 (2 Å) due to the (100) plane and small peaks due to the (110), (200), and (210) planes, confirming the hexagonal mesophase of the materials.[34] All these patterns are assigned to hexagonal symmetry.[28] XRD patterns of the calcined material prove that there is no collapse of structure or change of phase during calcination. This suggests that MCM-41 has good thermal stability after calcination.

The XRD patterns of the carbon nanotube samples with and without nickel particles are shown in Figure 2a,b, respectively. The patterns clearly show the carbon nanotubes are well-graphitized and pure. The carbon nanotubes with nickel catalyst shown in Figure 2a clearly show the primary peak of graphite at 26.2° corresponding to the plane of (002), and the next peak appears at 44.365° corresponding to the plane of (100). Similarly the primary peak of nickel due to the (111) plane appears at 44.505°, and the secondary peak of nickel at 51.844° due to the (200) plane was clearly seen in the spectrum. These XRD data coincide with the JCPDS data: 75-1621 of graphite and 04-0550 of nickel, respectively. The XRD pattern of carbon nanotubes after purification process is shown in Figure 2b, in which the nickel peaks are subdued in the chart, while the peaks of graphite are clearly shown.

(b) Nitrogen Adsorption Isotherms. BET surface area, pore volume, and pore size distribution (BJH method) of calcined

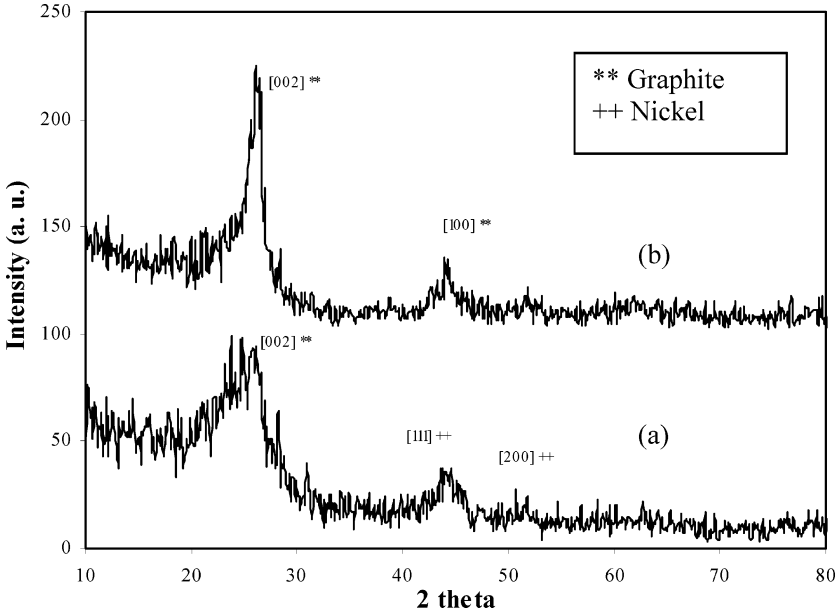

Figure 2. XRD patterns of the carbon nanotube samples (a) with nickel and (b) without nickel particles.

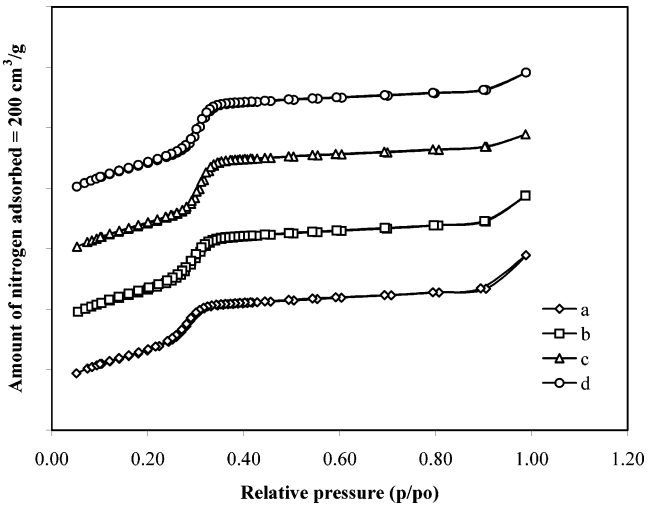

Figure 3. Adsorption isotherms of nitrogen on MCM-41 at 77 K: (a) Ni−MCM-41 (100), (b) Ni−MCM-41 (75), (c) Ni−MCM-41 (50), and (d) Ni−MCM-41 (25).

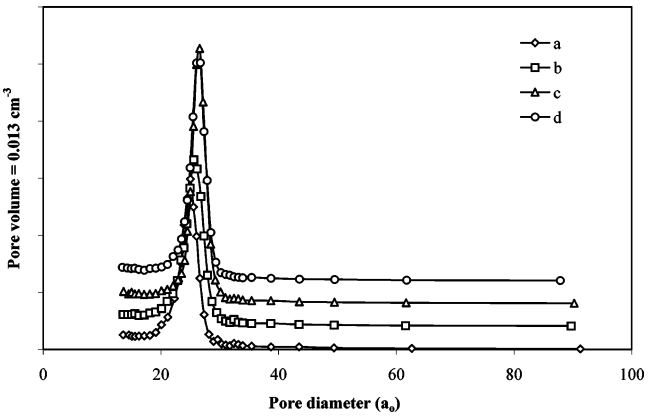

Figure 4. Pore size distributions in Ni−MCM-41 (adsorption isotherms): (a) Ni−MCM-41 (100), (b) Ni−MCM-41 (75), (c) Ni−MCM-41 (50), and (d) Ni−MCM-41 (25).

Ni−MCM-41 material are shown in Figure 3 and Figure 4, respectively, and their data are presented in Table 4. The isotherm of the sample shows a sharp inflection step at $p/p_0 \approx 0.3-0.4$, characteristic of capillary condensation of uniform mesoporous materials.[35] Three well-defined stages may be identified: (1) a slow increase in nitrogen uptake at low relative pressure, corresponding to monolayer−multilayer adsorption on the pore walls; (2) a sharp step at intermediate relative pressures, indicative of capillary condensation within mesopores; (3) a plateau with a slight calcination at high relative pressure associated with multilayer adsorption on the external surface of the crystal.[29] The isotherm further suggests that metal incorporation results in a shift to lower pore size (pore filling step at lower p/p_0) and that the decrease in pore size is greater at higher metal content. It is interesting to note from the isotherms that the presence of metal results in significant adsorption at high partial pressure (p/p_0). The point at which the inflection begins is related to the capillary condensation within the uniform mesopores and their diameter.

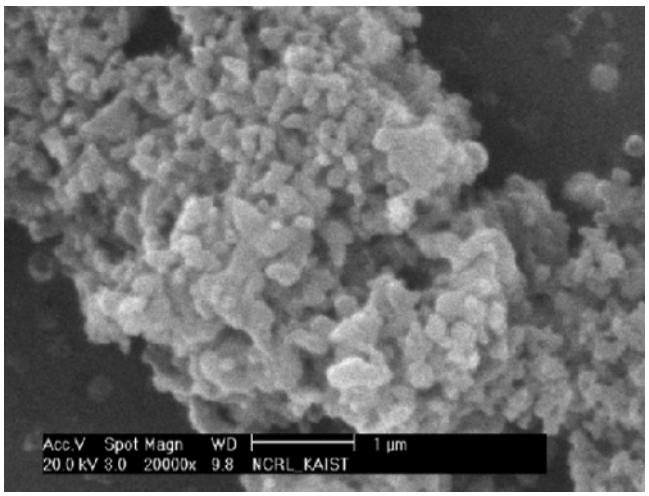

Figure 5. SEM image of the Ni−MCM-41 (100) sample.

(c) SEM and TEM. The SEM image of the Ni−MCM-41 (100) sample is presented in Figure 5. The image indicates a definite crystalline morphology, whereas the TEM image of the calcined sample, shown in Figure 6, shows the well-defined hexagonal array of channels characteristic of the MCM-41 structure.

The SEM image of purified CNTs prepared with mesoporous Ni−MCM-41 molecular sieves is shown in Figure 7. The SEM

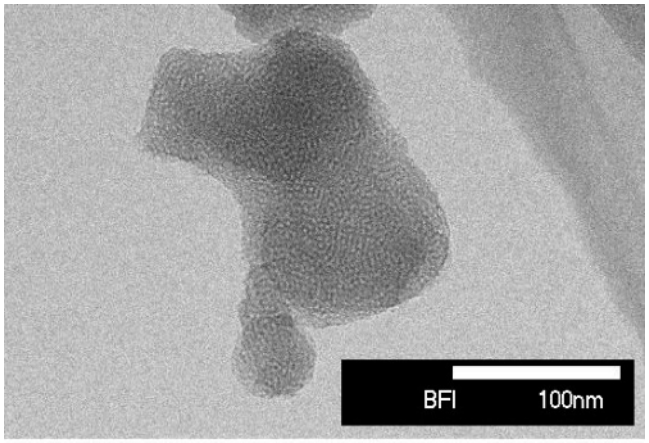

Figure 6. TEM image of the Ni−MCM-41 (100) sample.

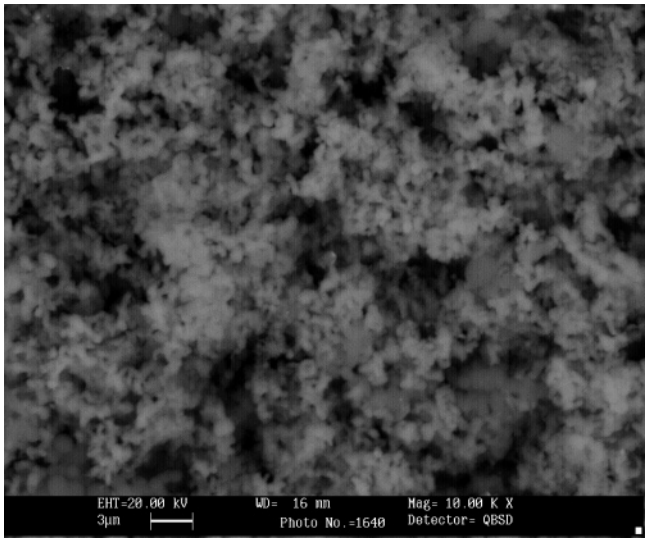

Figure 7. SEM image of carbon nanotubes.

image shows the morphology of CNTs, where a large number of CNTs along with traces of catalytic particles and amorphous carbon was found in the grown sample. This was further supported by observation through TEM, the images of which are shown in Figure 8a,b, respectively. The hollow core of the CNTs was large and the largest nanotubes found had a diameter of about 30 nm.

It is learned that the carbon precursor molecule will lift the metal particle, which is loosely bonded to the support, and the catalyst remains at the tip of the developing nanotubes. The TEM image displayed in Figure.8b indicates that some CNTs have bending structure, and at the close end of the tubes, the catalytic metal particles clearly exist, which suggests that the metal particles are responsible for the nucleation of the CNTs. Probably the nanotubes are formed by carbon dissolving in the metal particles and diffusing to the growing (002) graphite lattice planes, which are parallel to the metal surface. It could be shown by TEM image (Figure 8a) that the caps of the tubes are closed and metal particles are located in most cases at the tips of the tubes. From this it is very clear that the growth mechanism carbon nanotubes can be attributed to the "Tip Growth Model".[36,37]

(d) Raman Spectroscopy. We performed Raman spectroscopy in order to investigate the vibrational properties of the synthesized carbon structures, which also allow us to draw further conclusions about their crystallography or morphology. The Raman spectra of CNTs are shown in Figure 9. A typical

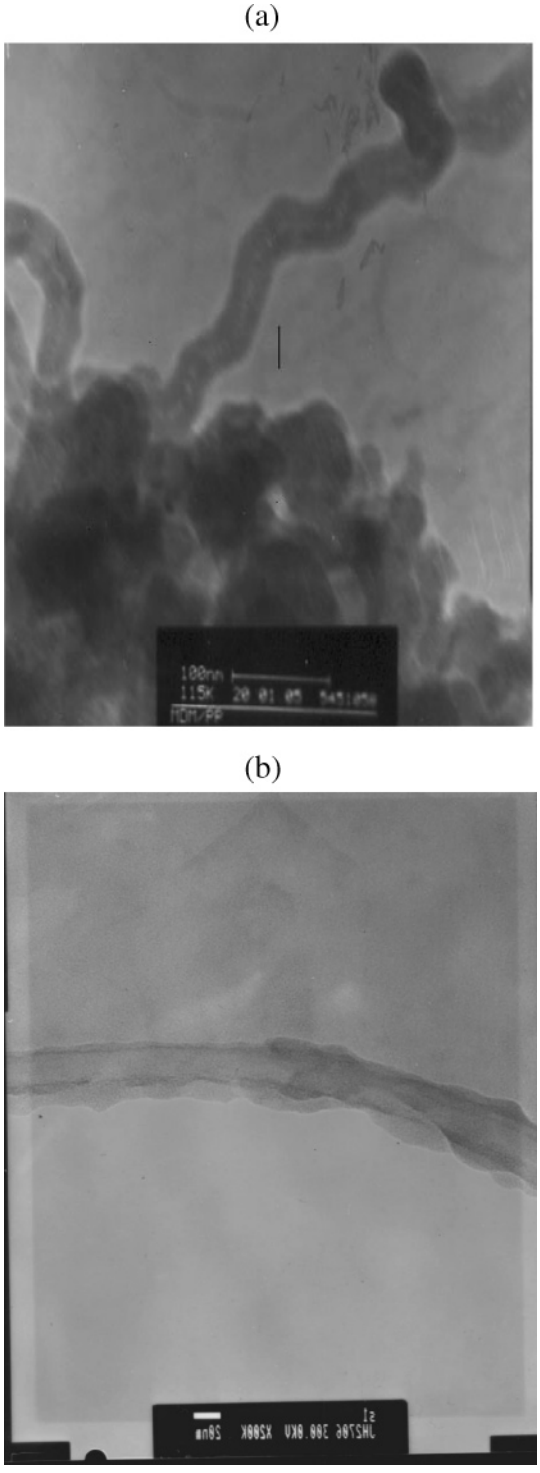

Figure 8. TEM images of carbon nanotubes: (a) tip growth and (b) bending structure.

Raman spectrum of CNTs is characterized by D-band, G-band, and, in some cases, a radial breathing mode (RBM). The D-band is associated with the amount of disordered carbon which occurs in the 1200−1400 cm^{-1} part of the spectrum,[38] particularly at 1345 cm^{-1}; the defects are related due to the graphene sheet and to the presence of amorphous carbon. The G-band reveals the intense tangential modes of CNTs and the good arrangement of the hexagonal lattice of graphite, which occurs in the high-frequency region of 1500−1600 cm^{-1}.[39] The RBM usually occurring in the low-frequency region (100−350 cm^{-1}) is generally considered as a special signature of SWNT. There are several RBM peaks in the range of 200−320 cm^{-1}

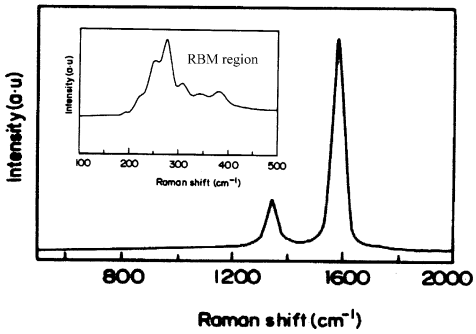

Figure 9. Raman spectra of carbon nanotubes.

corresponding to SWNT diameters in the range of 0.61−1.27 nm on the basis of the following relationship, $\omega_r = (223.75\ cm^{-1}\ nm)/(d/nm)$.[40] From this result, it is evident that under these reaction conditions Ni−MCM-41 (100) shows selective SWNT using acetylene as a carbon precursor.

Conclusions

Optimizing the reaction condition for maximum carbon yield resulted in 71.01% carbon yield using Ni−MCM-41 (100) at 750 °C for 10 min at nitrogen and acetylene flow rates of 140 and 60 mL/min, respectively. The TEM studies show the formation of CNTs, and results clearly indicate that the metal particles are at the tip of the CNTs, confirming the tip growth mechanism. The nickel isomorphously substituted for silica in the MCM-41 framework was found to be stable under severe reaction conditions, allowing slow reduction and nucleation of metallic clusters for production of large carbon yields at high reaction temperatures with high selectivity for SWNTs. This study suggested that the mesoporous molecular sieves could be a promising catalytic template for synthesizing CNTs.

Acknowledgment

The authors would like to thank the Board of Research in Nuclear Science (Grant 2002/34/13-BRNS/443) for providing financial support.

Literature Cited

(1) Iijima, S. *Nature (London)* **1991**, *354*, 56.
(2) Frank, S.; Poncharal, P.; Wang, Z. L.; deHeer, W. A. *Science (Washington, D. C.)* **1998**, *280*, 1744.
(3) Dillon, A. C.; Jones, K. M.; Bekkedahl, T. A.; Kiang, C. H.; Bethune, D. S.; Heben, M. J. *Nature (London)* **1997**, *386*, 377.
(4) Fan, S.; Chapline, M. G.; Franklin, N. R.; Tombler, T. W.; Cassell, A. M.; Dai, H. J. *Science (Washington, D. C.)* **1999**, *283*, 512.
(5) Kim, P.; Lieber, C. M. *Science (Washington, D. C.)* **1999**, *286*, 2148.
(6) Nutzenadel, C.; Zuttel, A.; Chartouni, D.; Schlapbach, L. *Electrochem. Solid State. Lett.* **1999**, *2*, 30.
(7) Rajalakshmi, N.; Dhathathreyan, K. S.; Govindaraj, A.; Satishkumar, B. C. *Electrochim. Acta* **2000**, *45*, 4511.
(8) Dresselhaus, M. S.; Williams, K. A.; Eklund, P. C. *Mater. Res. Soc. Bull.* **1999**, *2*, 45.
(9) Saito, R.; Dresselhaus, M. S. *Physical Properties of Carbon Nanotubes*; Imperial College Press: London, 1998.
(10) Zhang, Z. J.; Wei, B. Q.; Ramnath, G.; Ajayan, P. M. *Appl. Phys. Lett.* **2000**, *77*, 3764.
(11) Nerushev, O. A.; Dittmar, S.; Morjan, R. E.; Rohmund, F.; Campbell, E. E. B. *J. Appl. Phys.* **2003**, *93*, 4185.
(12) Bethune, D. S.; Kiang, C. H.; deVries, M. S.; Gorman, G.; Savoy, R.; Vazquez, J.; Beyers, R. *Nature (London)* **1993**, *363*, 605.
(13) Guo, T.; Nikolaev, P.; Thess, V.; Colbert, D. T.; Smalley, R. E. *Chem. Phys. Lett.* **1995**, *243*, 49.
(14) Yudasaka, M.; Kituchi, R.; Matsui, V.; Ohki, Y.; Yoshimura, S.; Ota, E. *Appl. Phys. Lett.* **1995**, *67*, 2477.
(15) Geng, J.; Singh, G.; Shepard, D. S.; Shaffer, M. S. P.; Johnson, B. F. G.; Windle, A. H. *Chem. Commun. (Cambridge)* **2002**, 2666.
(16) Colomer, J. F.; Stephan, C.; Lefrant, S.; Van Tendeloo, G.; Willems, L.; Konya, Z.; Fonseca, A.; Laurent, Ch.; Nagy, J. B. *Chem. Phys. Lett.* **2000**, *317*, 83.
(17) Kong, J.; Cassell, A. M.; Dai, H. *Chem. Phys. Lett.* **1998**, *292*, 567.
(18) Ago, H.; Imamura, S.; Okazaki, T.; Saito, T.; Yumura, M.; Tsuji, M. *J. Phys. Chem. B* **2005**, *109*, 10035.
(19) Hata, K.; Futaba, D. N.; Mizuno, K.; Namai, T.; Yumura, M.; Iijima, S. *Science (Washington, D. C.)* **2004**, *306*, 1362.
(20) Lyu, S. C.; Liu, B. C.; Lee, S. H.; Park, C. Y.; Kang, H. K.; Yang, C. W.; Lee, C. J. *J. Phys. Chem. B* **2004**, *108*, 1613.
(21) Amama, P. B.; Lim, S.; Ciupura, D.; Yang, Y.; Pfefferle, L.; Haller, G. L. *J. Phys. Chem. B* **2005**, *109*, 2645.
(22) Liu, B. C.; Lyu, S. C.; Jung, S. I.; Kang, H. K.; Yang, C. W.; Park, J. W.; Park, C. Y.; Lee, C. J. *Chem. Phys. Lett.* **2004**, *383*, 104.
(23) Lacerda, R. G.; The, A. S.; Yang, M. H.; Teo, K. B. K.; Rupesinghe, N. L.; Dalal, S. H.; Koziol, K. K. K.; Roy, D.; Amaratunga, G. A. J.; Milne, W. I.; Chhowalla, M.; Hasko, D. G.; Wyczisk, F.; Legagneux, P. *Appl. Phys. Lett.* **2004**, *84*, 269.
(24) Rao, C. N. R.; Satishkumar, B. C.; Govindaraj, A.; Nath, M. *ChemPhysChem* **2001**, *2*, 78.
(25) Lim, S.; Ciupura, D.; Pak, C.; Dobek, F.; Chen, Y.; Harding, D.; Pfefferle, L.; Haller, G. L. *J. Phys. Chem. B* **2005**, *107*, 11048.
(26) Ciupura, D.; Chen, Y.; Lim, S.; Haller, G. L.; Pfefferle, L. *J. Phys. Chem. B* **2004**, *108*, 503.
(27) Jeong, H. J.; An, K. H.; Lim, S. C.; Park, M. S.; Chang, J. S.; Park, S. E.; Eum, S. J.; Yang, C. W.; Park, C. Y.; Lee, Y. H. *Chem. Phys. Lett.* **2003**, *306*, 263.
(28) Beck, J. S.; Vartuli, J. C.; Ruth, W. J.; Leonowicz, M. E.; Kresge, C. T.; Schmidt, K. D.; Chu, C. T. W.; Olson, D. H.; Sheppard, E. W.; McCullen, S. B.; Hggins, J. B.; Schlenker, J. L. *J. Am. Chem. Soc.* **1992**, *114*, 10834.
(29) Corma, A. *Chem. Rev.* **1997**, *97*, 2373.
(30) Li, Y.; Kim, W.; Zhang, Y.; Rolandi, M.; Wang, D.; Dai, H. *J. Phys. Chem. B* **2001**, *105*, 11424.
(31) Somanathan, T.: Pandurangan, A.: Sathiyamoorthy, D. *J. Mol. Catal. A: Chem.* **2006**, *256*, 193.
(32) Urbán, M.; Méhn, D.; Kónya, Z.; Kiricsi, I. *Chem. Phys. Lett.* **2002**, *359*, 95.
(33) Rostrup-Nielson, J.; Trimm, D. L. *J. Catal.* **1977**, *48*, 155.
(34) Pauly, T. R.; Lu, Y.; Pinnavaia, T. J.; Billinge, S. J. L.; Rieker, T. P. *J. Am. Chem. Soc.* **1999**, *121*, 8835.
(35) Gregg, S. J.; Sing, K. S. W. *Adsorption, Surface Area and Porosity*; Academic Press: London, 1982.
(36) Oberlin, A.; Endo, M.; Koyama, T. *J. Cryst. Growth* **1976**, *32*, 335.
(37) Kanzow, H.; Schmalz, A.; Ding, A. *Chem. Phys. Lett.* **1998**, *295*, 525.
(38) Dillon, R. O.; Woollam, J. A.; Katkanant, V. *Phys. Rev. B* **1984**, *29*, 3482.
(39) Tuinstra, F.; Koenig, J. L. *J. Chem. Phys.* **1970**, *53*, 1126.
(40) Bandow, S.; Asaka, S.; Saito, Y.; Rao, A. M.; Grigorian, L.; Richter, E.; Eklund, P. C. *Phys. Rev. Lett.* **1998**, *80*, 3779.

Received for review May 25, 2006
Revised manuscript received September 20, 2006
Accepted October 5, 2006

IE060663A